Proceedings of IAM, V.13, N.1, 2024, pp.3-34
DOI: 10.30546/2225-0530.13.1.2024.024.

B-SPLINE BIORTHOGONAL WAVELET MULTIGRID METHOD FOR THE NUMERICAL SOLUTION OF COUPLE STRESS FULL REYNOLDS EQUATION

S.C. Shiralashetti[1], A.B. Deshi[2*], M.H. Kantli[3]

[1]Department of Mathematics, Karnatak University, Dharwad, India-580003
[2]Department of Mathematics, KLECET, Chikodi, India-591201
[3]Department of Mathematics, BVV's BGMIT, Mudhol, India-587313

Abstract: The theory of wavelets provides an extremely useful mathematical tool for hierarchically decomposing function efficiently and correctly. A wavelet representation of functions consists of approximation coefficients and detail coefficients that influence the function at various scales. In this paper, B-spline biorthogonal wavelet multigrid method is proposed for the numerical solution of couple stress full Reynolds equation. The performance of proposed scheme is better than the existing ones in terms of super convergence with low computational time, is shown for elliptic partial differential equation first and then applied to Reynolds equation. The test problems are presented to demonstrate the versatility and applicability of the proposed method.

Keywords: B-spline biorthogonal wavelets, Multigrid method, Elliptic partial differential equations, Reynolds equation.

AMS Subject Classification: 65T60, 65N06, 65N55, 76D08.

1. Introduction

In the numerical research, wavelets are used as well-organized tool for the rapid numerical applications in the differential equations [11-13, 15, 27, 28]. They are generally applied in engineering field namely signal analysis, image processing, etc [1-3, 18, 36]. Consequently, the development of multi-resolution analysis and the fast wavelet transforms by Avudainayagam and Vani (2004) and Bujurke et al. (2006, 2007a and 2007b) led to extensive research in the wavelet multigrid (WMG) schemes for the numerical solution of certain differential equations arising in fluid dynamics. Shiralashetti et al. (2017) had proposed the modified wavelet multigrid method (MWMG) for the solution of boundary value problems. Extension to this, the same procedure has applied for the numerical solution of modified Reynolds equation (Shiralashetti, Kantli and Deshi Forthcoming). Beylkin, Coifman and Rokhlin (1991) observed that wavelet decomposition can be used to approximate the systems of certain different types of highly sparse matrices.

The biorthogonal wavelets reveal both higher compression factors and faster execution than the corresponding orthogonal wavelets at comparable accuracy. Thus, they are highly competitive, alternative to Daubechies wavelet and Coiflets for the applications in numerical approximation. For the finest results, the

wavelets should have several vanishing moments, good advantages and a support as small as possible. Orthogonal wavelets are expected to give the best compression ratio, while biorthogonal wavelets lead to faster decomposition algorithms at slightly reduced compression. Extension to (Shiralashetti, Kantli and Deshi Forthcoming), the main objective of this paper is to introduce the B-spline biorthogonal wavelet multigrid (BBWMG) schemes for the numerical solution of couple stress full Reynolds equation.

Traditionally, the studies of squeeze film motion focus upon the characteristics of porous bearings lubricated with a Newtonian fluid as lubricant in which the fluid is assumed to obey the Newtonian postulate that the stress tensor is directly proportional to the deformation tensor. However, with the growth of modern machine equipments, the increasing use of non-Newtonian fluid as lubricants are becoming of great interest. Among these theories, the Stokes (1966) micro continuum theory is the simplest generalization of the classical theory of fluids, which allows for polar effects such as the presence of couple stresses and body couples in a continuous medium. The classical Newtonian theory will not predict the accurate flow behavior of fluid suspensions, especially when the clearance in the bearing is comparable with average size of the lubricant additives. The consideration of couple stress in addition to the classical Cauchy stress has led to the current development of theories of fluid micro continua. The Stokes couple stress theory of fluids defines the rotation field in terms of the velocity fields. Several researchers for example, Luhmar (2005), Naduvinamani, Hiremath and Gurubaswaraj (2001a) used this couple stress fluid theory for the study of different bearing systems. Ramanaih and Sarkar (1978 and 1979) studied the effect of couple stress on the squeeze film between two parallel rectangular plates with infinite lengths and that between two parallel rectangular plates with finite size. Lin, Lu and Chang (2003) worked on the derivation of dynamic couple stress Reynolds equation of sliding squeezing surfaces and numerical solution of plane inclined slider bearing. Recently the contribution in this regard includes finite difference method (Naduvinamani and Marali 2007; Naduvinamani and Patil 2009), finite element method and multigrid (MG) method, etc.

The multigrid scheme is largely applicable in increasing the efficiency of the iterative methods to solve system of algebraic equations. It is a well-founded numerical method for solving system of equations for an approximating the given differential equation. Nowadays, it is recognized that MG iterative solver is highly efficient for the differential equations, introduced by Brandt (1977). For a detailed treatment of MG is given in Briggs, Henson and McCormick (2000). An introduction of MG is found in Hackbusch and Trottenberg (1982), Wesseling (1992) and Trottenberg, Oosterlee and Schuller (2001). The ill-conditioned matrices are arising in the solution of system of algebraic equations. The suitable remedy is multigrid schemes for such matrices. Matrices are dense with non-smooth diagonal and smooth away from the diagonal. This smoothness of the matrix transforms into smallness in wavelet transform and facilitates in the design or construction of efficient multigrid scheme using biorthogonal discrete wavelet transform (BDWT).

Sweldens (1994) highlighted effectively the construction of biorthogonal wavelet filters for the solution of large class of ill-conditioned system. The BDWT matrix designed and implemented by Ruch and Fleet (2009) for decomposition and reconstruction of the given signals and images. Shiralashetti, Kantli and Deshi (2018) and Shiralashetti, Angadi and Deshi (2019) proposed the Biorthogonal wavelet based full-approximation schemes for the numerical solution of elasto-hydrodynamic lubrication problems and parabolic partial differential equations. Extension to this, we introduced restriction and prolongation operators, respectively using decomposition and reconstruction matrices in the implementation of BBWMG schemes for the numerical solution of couple stress full Reynolds equation.

This paper is follows as, Preliminaries of biorthogonal wavelets are given in section 2. Section 3 deals with the formulation of the problem. Section 4 describes the method of solution using intergrid operators. Numerical solutions of the test problems are presented in section 5. Section 6 represents the results and discussion. Finally, conclusions of the proposed work are discussed in section 7.

2. Biorthogonal wavelets

Biorthogonal wavelets are the important things in many profitable claims like signal processing, finger print image compression. In various filtering applications, we need filters with symmetrical coefficients to accomplish linear phase. None of the orthogonal wavelet systems apart from Haar are having symmetrical coefficients. But Haar is too insufficient for countless practical applications. Biorthogonal wavelet system can be planned to have this property. To understand the entire theory more let us primarily consider some biorthogonal filters and construct corresponding scaling functions and wavelet functions. Spline based biorthogonal wavelet systems are more easy to construct (Soman and Ramachandran 2005).

2.1. B-spline biorthogonal wavelets/Cohen-Daubechies-Feauveau (CDF) wavelets

We know that, the splines of any order follow scaling relation. But their integer translates are not orthogonal (apart from Haar). The generalized scaling relation of spline $N_m(x)$,

$$N_m(x) = \sum_{i=0}^{m} p_i N_m(2x-m) \tag{1}$$

where

$$p_i = \frac{1}{2^{m-1}} \binom{m}{i}. \tag{2}$$

Therefore, we find the dual scaling function.

Let, $\phi(x) = N_2(x)$ and $V_0 \equiv \operatorname{span}_m\{N_2(x-m)\}$. (3)

Let us take a matching $\tilde{\phi}(x)$ whose scaling relation have five continuous non-zero coefficients. Support of $\tilde{\phi}(x)$ is 5. We could have preferred any positive odd number (other than 3) the support of its dual, that is $\phi(x)$, since $\int \phi(x)\tilde{\phi}(x-m)dx = \delta_{m,0}$. For the spline scaling function $N_2(x)$, scaling function coefficients are 1/2, 1, 1/2. However, these are not normalized. We know that the sum of normalized coefficients is $\sqrt{2}$, which follows from the constraint that $\int \phi(x)dx = 1$.

$$a\left(\frac{1}{2}+1+\frac{1}{2}\right) = \sqrt{2} \Rightarrow a = \frac{1}{\sqrt{2}}. \tag{4}$$

Therefore, normalized coefficients of $\phi(x) = N_2(x)$ are: $\frac{1}{2\sqrt{2}}, \frac{1}{\sqrt{2}}, \frac{1}{2\sqrt{2}}$.

Let $\tilde{h}_f(0), \tilde{h}_f(1), \tilde{h}_f(2), \tilde{h}_f(3), \tilde{h}_f(4)$ be the normalized scaling filter coefficients of $\tilde{\phi}(x)$. Since $\int \phi(x)\tilde{\phi}(x-m)dx = \delta_{m,0}$, we have

$$\sum_n h_f(n)\tilde{h}_f(n-2m) = \delta_{m,0}. \tag{5}$$

This is the main relation which decides $\tilde{\phi}(x)$.
In the orthogonal case, we have

$$\sum_n h_f(n)h_f(n-2m) = \delta_{m,0}, \tag{6}$$

i.e., $h_f(n)$ is orthogonal to even translate of itself. Here $\tilde{h}_f$ is orthogonal to h_f, thus the name biorthogonal. Eq. (5) is the key to understanding of the B-spline biorthogonal wavelets. Assume $\tilde{h}_f(n)$ is non-zero when $\tilde{N}_1 \le n \le \tilde{N}_2$ and $h(n)$ is non-zero when $N_1 \le n \le N_2$. Eq. (5) implies that,

$$N_2 - \tilde{N}_1 = 2m+1 \text{ and } \tilde{N}_2 - N_1 = 2\tilde{m}+1,\ m,\ \tilde{m} \in Z. \tag{7}$$

In the orthogonal case, this shrinks to the well-known fact that the length of h_f has to be even. Eq. (5) also implies that the difference between the lengths of $\tilde{h}_f$ and h_f must be even. Thus, their length must be either even or odd. Now, try to visualize Eqs. (5) and (7). The arranging of scaling function coefficients is main thing. If Eq. (7) is not satisfied then it is not possible to get an achievable solution for $\tilde{h}_f(m)$ coefficients. Many applications require symmetric scaling function coefficients. For symmetry, we need $\tilde{h}_f(0) = \tilde{h}_f(4)$ and $\tilde{h}_f(1) = \tilde{h}_f(3)$. Now, apply these conditions on coefficients.

For $\int \tilde{\phi}(x)dx = 1$, we have the condition

$$\sum_m \tilde{h}_f(m) = \sqrt{2} \tag{8}$$

which implies $2\tilde{h}_f(0) + 2\tilde{h}_f(1) + \tilde{h}_f(2) = \sqrt{2}$.

For $m = 0$, Eq. (5) gives

$$\frac{1}{2\sqrt{2}}\tilde{h}_f(1) + \frac{1}{\sqrt{2}}\tilde{h}_f(2) + \frac{1}{2\sqrt{2}}\tilde{h}_f(1) = 1 \Rightarrow \frac{1}{\sqrt{2}}\tilde{h}_f(1) + \frac{1}{\sqrt{2}}\tilde{h}_f(2) = 1. \tag{9}$$

For $m = 1$, Eq. (5) becomes,

$$\frac{1}{2\sqrt{2}}\tilde{h}_f(1) + \frac{1}{\sqrt{2}}\tilde{h}_f(0) = 0 \Rightarrow \frac{1}{2}\tilde{h}_f(1) + \tilde{h}_f(0) = 0. \tag{10}$$

For $m = -1$, that also gives the same condition as given in Eq. (10), since we assumed that $\tilde{h}_f(m)$ are symmetric.

Since $\tilde{\phi}(x) \perp \Psi(x)$, we have

$$\Psi(x) = \sum_{m=0}^{L_1-1} (-1)^n \tilde{h}_f(L_1 - m - 1)\tilde{\phi}(2x - m), \tag{11}$$

i.e. $\Psi(x)$ function depends on $\tilde{h}_f(m)$, such that $\int \Psi(x)dx = 0$. This requires that $\sum_{m=0}^{L_1-1} (-1)^n \tilde{h}(L_1 - m - 1) = 0$ which is the vanishing moment condition, where L_1 is length of the filter. Thus, we have

$$\tilde{h}_f(4) - \tilde{h}_f(3) + \tilde{h}_f(2) - \tilde{h}_f(1) + \tilde{h}_f(0) = 0 \Rightarrow 2\tilde{h}_f(0) - 2\tilde{h}_f(1) + \tilde{h}_f(2) = 0. \tag{12}$$

By combining all conditions, we have

i. Normality: $2\tilde{h}_f(0) + 2\tilde{h}_f(1) + \tilde{h}_f(2) = \sqrt{2}$.

ii. Biorthogonality: For $m = 0$, $\frac{1}{\sqrt{2}}\tilde{h}_f(1) + \frac{1}{\sqrt{2}}\tilde{h}_f(2) = 1$ and

For $m = 1$, $\frac{1}{2}\tilde{h}_f(1) + \tilde{h}_f(0) = 0$.

iii. .Vanishing moment: $2\tilde{h}_f(0) - 2\tilde{h}_f(1) + \tilde{h}_f(2) = 0$.

Solving the above equations, we get

$$\tilde{h}_f(0) = \frac{-\sqrt{2}}{8}, \quad \tilde{h}_f(1) = \frac{\sqrt{2}}{4}, \quad \tilde{h}_f(2) = \frac{3\sqrt{2}}{4}.$$

By symmetry, $\tilde{h}_f(3) = \frac{\sqrt{2}}{4}$, $\tilde{h}_f(4) = \frac{-\sqrt{2}}{8}$. Ruch and Fleet (2009) had built a biorthogonal structure called dual multi-resolution analysis that allows for the construction of symmetric scaling filters and that can incorporate spline functions.

They used instead of scaling (h_f) and wavelet (g_f) filters, the new construct yields scaling $(\tilde{h}_f)$ and wavelet $(\tilde{g}_f)$ filters as decomposition and reconstruction. Instead of a single scaling function $\phi(x)$ and wavelet function $\Psi(x)$, the dual multi-resolution analysis requires a pair of scaling functions $\phi(x)$ and $\tilde{\phi}(x)$ related by a duality condition similarly, a pair of wavelet functions $\Psi(x)$ and $\tilde{\Psi}(x)$. To construct the BDWT matrix, follow the same procedure as used to build the orthogonal discrete wavelet transform matrix. Due to excellent properties of biorthogonality and minimum compact support, CDF wavelets can be useful and convenient, providing guaranty of convergence and accuracy of the approximation in a wide variety of situations.

In this paper, we use CDF (2, 2) filter coefficients which are, Low pass filter coefficients:

$$h_{f-1} = -\frac{\sqrt{2}}{8},\ h_{f0} = \frac{\sqrt{2}}{4},\ h_{f1} = \frac{3\sqrt{2}}{4},\ h_{f2} = \frac{\sqrt{2}}{4},\ h_{f3} = -\frac{\sqrt{2}}{8}.$$

High pass filter coefficients: $g_{f-1} = \frac{\sqrt{2}}{4},\ g_{f0} = -\frac{\sqrt{2}}{2},\ g_{f1} = \frac{\sqrt{2}}{4}$ for decomposition matrix.

Low pass filter coefficients: $\tilde{h}_{f-1} = g_{f1},\ \tilde{h}_{f0} = -g_{f0},\ \tilde{h}_{f1} = g_{f-1}$. High pass filter coefficients: $\tilde{g}_{f-1} = -h_{f3},\ \tilde{g}_{f0} = h_{f2},\ \tilde{g}_{f1} = -h_{f1},\ \tilde{g}_{f2} = h_{f0},\ \tilde{g}_{f3} = -h_{f-1}$ for reconstruction matrix.

2.2. Biorthogonal discrete wavelet transforms (BDWT) matrix

The matrix formulation of the BDWT plays an important role in the biorthogonal wavelet method for the numerical computations. We know about the BDWT matrix and its applications in the wavelet method and are given as,

Decomposition matrix:

$$Dw = \begin{pmatrix} h_{f0} & h_{f1} & h_{f2} & h_{f3} & 0 & 0 & \dots & 0 & 0 & h_{f-1} \\ g_{f0} & g_{f1} & 0 & 0 & 0 & 0 & \dots & 0 & 0 & g_{f-1} \\ 0 & h_{f-1} & h_{f0} & h_{f1} & h_{f2} & h_{f3} & \dots & 0 & 0 & 0 \\ 0 & g_{f-1} & g_{f0} & g_{f1} & 0 & 0 & \dots & 0 & 0 & 0 \\ \vdots & \ddots & & \dots & & & \dots & & 0 & 0 \\ h_{f2} & h_{f3} & 0 & 0 & \dots & \dots & 0 & h_{f-1} & h_{f0} & h_{f1} \\ 0 & 0 & 0 & 0 & \dots & \dots & 0 & g_{f-1} & g_{f0} & g_{f1} \end{pmatrix}_{N\times N}$$ and

Reconstruction matrix:

$$Rw = \begin{pmatrix} \tilde{h}_{f0} & \tilde{h}_{f1} & 0 & 0 & 0 & 0 & \dots & 0 & 0 & \tilde{h}_{f-1} \\ \tilde{g}_{f0} & \tilde{g}_{f1} & \tilde{g}_{f2} & \tilde{g}_{f3} & 0 & 0 & \dots & 0 & 0 & \tilde{g}_{f-1} \\ 0 & \tilde{h}_{f-1} & \tilde{h}_{f0} & \tilde{h}_{f1} & 0 & 0 & \dots & 0 & 0 & 0 \\ 0 & \tilde{g}_{f-1} & \tilde{g}_{f0} & \tilde{g}_{f1} & \tilde{g}_{f2} & \tilde{g}_{f3} & \dots & 0 & 0 & 0 \\ \vdots & \ddots & & \dots & & \dots & & 0 & 0 & 0 \\ 0 & 0 & 0 & 0 & \dots & \dots & 0 & \tilde{h}_{f-1} & \tilde{h}_{f0} & \tilde{h}_{f1} \\ \tilde{g}_{f2} & \tilde{g}_{f3} & 0 & 0 & \dots & \dots & 0 & \tilde{g}_{f-1} & \tilde{g}_{f0} & \tilde{g}_{f1} \end{pmatrix}_{N\times N}.$$

Using these matrices, we introduced restriction and prolongation operators, respectively as same as the restriction and prolongation operators of the multigrid scheme and the detailed procedure is explained in section 4.

2.3. Modified biorthogonal discrete wavelet transform (MBDWT) matrix

Here, MBDWT matrix is developed alike BDWT matrix in which by adding rows and columns consecutively with diagonal element as 1, which is built as,
Modified decomposition matrix:

$$MDw = \begin{pmatrix} h_{f0} & 0 & h_{f1} & 0 & h_{f2} & 0 & h_{f3} & 0 & \dots & 0 & 0 & 0 & h_{f-1} & 0 \\ 0 & 1 & 0 & 0 & \dots & \dots & & \dots & 0 & 0 & 0 & 0 & 0 & \\ g_{f0} & 0 & g_{f1} & 0 & \dots & \dots & & \dots & 0 & 0 & 0 & g_{f-1} & 0 & \\ 0 & 0 & 0 & 1 & 0 & 0 & \dots & & \dots & 0 & 0 & 0 & 0 & 0 \\ \vdots & & \ddots & & \dots & & \dots & & \ddots & & \vdots & & & \\ h_{f2} & 0 & h_{f3} & 0 & \dots & 0 & 0 & 0 & h_{f-1} & 0 & h_{f0} & 0 & h_{f1} & 0 \\ 0 & 0 & \dots & & \dots & & \dots & & 0 & 0 & 1 & 0 & 0 & \\ 0 & 0 & 0 & 0 & \dots & \dots & 0 & g_{f-1} & 0 & g_{f0} & 0 & g_{f1} & 0 & \\ 0 & 0 & \dots & & \dots & & \dots & & 0 & 0 & 0 & 0 & 1 & \end{pmatrix}_{N\times N}$$

and
Modified reconstruction matrix:

$$MRw = \begin{pmatrix} \tilde{h}_{f0} & 0 & \tilde{h}_{f1} & 0 & 0 & 0 & 0 & \dots & 0 & 0 & \tilde{h}_{f-1} & 0 \\ 0 & 1 & 0 & 0 & \dots & & \dots & & 0 & 0 & 0 & 0 \\ \tilde{g}_{f0} & 0 & \tilde{g}_{f1} & 0 & \tilde{g}_{f2} & 0 & \tilde{g}_{f3} & \dots & 0 & 0 & \tilde{g}_{f-1} & 0 \\ 0 & 0 & 0 & 1 & 0 & & \dots & & 0 & 0 & 0 & 0 \\ \vdots & & \ddots & & & \dots & & \dots & & \ddots & \vdots & \\ 0 & 0 & & \dots & & 0 & \tilde{h}_{f-1} & 0 & \tilde{h}_{f0} & 0 & \tilde{h}_{f1} & 0 \\ 0 & 0 & 0 & \dots & & \dots & & \dots & 0 & 1 & 0 & 0 \\ \tilde{g}_{f2} & 0 & \tilde{g}_{f3} & \dots & 0 & 0 & 0 & \tilde{g}_{f-1} & 0 & \tilde{g}_{f0} & 0 & \tilde{g}_{f1} & 0 \\ 0 & 0 & 0 & \dots & & \dots & & \dots & 0 & 0 & 0 & 1 \end{pmatrix}_{N\times N}.$$

Using these matrices, a new restriction and prolongation operators are introduced, respectively as same as the restriction and prolongation operators of the multigrid scheme and the detailed procedure is explained in section 4.

3. Formulation of the problem

The fundamental equations derived by Stokes (1966) for the motion of an incompressible couple stress fluid, in the absence of body forces and body moments are

$$\rho \frac{D\vec{q}}{Dt} = -\nabla p + \mu \nabla^2 \vec{q} - \eta \nabla^4 \vec{q} \tag{13}$$

$$\nabla \vec{q} = 0 \tag{14}$$

where ρ is the density, $\vec{q}$ is the velocity vector, p is the pressure, μ is the Newtonian shear viscosity and η is a material constant accounting for the couple stress property. The ratio $\left(\frac{\eta}{\mu}\right)$ has the dimensions of the length squared and hence the dimension of $\sqrt{\frac{\eta}{\mu}}$ characterizes the material length of the couple stress fluid.

It consists of porous slider with sliding velocity U including the effect of the squeezing action $\frac{\partial h}{\partial t}$, $h_1(t)$ is the inlet film thickness and the outlet film thickness is $h_0(t)$. The porous region is assumed to be homogenous and isotropic and the lubricant is incompressible couple stress fluid. Pinkus and Sternlicht (1961) observed that under the usual assumptions of the hydrodynamic lubrication, applicable for thin films, the Eqs. (13) and (14) of motion take the form;

$$\frac{\partial p}{\partial x} = \mu \frac{\partial^2 u}{\partial y^2} - \eta \frac{\partial^4 u}{\partial y^4}, \tag{15}$$

$$\frac{\partial p}{\partial z} = \mu \frac{\partial^2 w}{\partial y^2} - \eta \frac{\partial^4 w}{\partial y^4}, \tag{16}$$

$$\frac{\partial p}{\partial y} = 0, \tag{17}$$

$$\frac{\partial u}{\partial x} + \frac{\partial v}{\partial y} + \frac{\partial w}{\partial z} = 0. \tag{18}$$

The relevant boundary conditions for velocity components are

(i) At the upper solid surface $(y = h)$

$$u = w = 0 \tag{19}$$

$$v = \frac{\partial h}{\partial t} \text{ (squeezing velocity)} \tag{20}$$

$$\frac{\partial^2 u}{\partial y^2} = \frac{\partial^2 w}{\partial y^2} = 0 \text{ . (vanishing of couple stresses)} \tag{21}$$

(ii) At the fluid porous interface $(y = 0)$

$$v = -v_1 \text{ , (continuity of vertical component)} \tag{22}$$

$$\frac{\partial^2 u}{\partial y^2} = \frac{\partial^2 w}{\partial y^2} = 0 \text{ . (vanishing of couple stresses)} \tag{23}$$

The solution of Eqs. (15) and (16) subject to boundary conditions (19), (21) and (23) is obtained as

$$u = \frac{1}{2\mu} \frac{\partial p}{\partial x} \left[y^2 - hy + 2l^2 \left\{ 1 - \frac{\cosh\left(\frac{2y - h}{2l} \right)}{\cosh\left(\frac{h}{2l} \right)} \right\} \right] \tag{24}$$

$$w = \frac{1}{2\mu} \frac{\partial p}{\partial z} \left[y^2 - hy + 2l^2 \left\{ 1 - \frac{\cosh\left(\frac{2y - h}{2l} \right)}{\cosh\left(\frac{h}{2l} \right)} \right\} \right] \tag{25}$$

where $l = \left(\frac{\eta}{\mu} \right)^{1/2}$ couple stress parameter.

Integrating the continuity Eq. (18) with respect to y over the film thickness gives;

$$-\int_{y=0}^{h} \frac{\partial v}{\partial y} dy = \int_{y=0}^{h} \left(\frac{\partial u}{\partial x} + \frac{\partial w}{\partial z} \right) dy. \tag{26}$$

By replacing the velocity components u and w with their expressions given in Eqs. (24) and (25), and also using the boundary conditions (20) and (22), the Eq. (26) gives the modified Reynolds type equation in the form

$$\frac{\partial}{\partial x}\left[f(h,l)\frac{\partial p}{\partial x}\right]+\frac{\partial}{\partial z}\left[f(h,l)\frac{\partial p}{\partial z}\right]=12\mu\frac{\partial h}{\partial t}+12\mu(v_1)_{y=0}, \tag{27}$$

where

$$f(h,l)=h^3-12l^2h+24l^3\tanh\left(\frac{h}{2l}\right). \tag{28}$$

The flow of couple stress fluid in a porous matrix is governed by the modified form of Darcy law which accounts for polar effects given by Naduvinamani, Hiremath, and Gurubasawaraj (2001b)

$$u_1=\frac{-k}{\mu(1-\beta)}\frac{\partial p^*}{\partial x}, \tag{29}$$

$$v_1=\frac{-k}{\mu(1-\beta)}\frac{\partial p^*}{\partial y}, \tag{30}$$

$$w_1=\frac{-k}{\mu(1-\beta)}\frac{\partial p^*}{\partial z}, \tag{31}$$

where u_1, v_1, w_1 are modified Darcy velocity components along x, y, z directions, respectively, p^* is the pressure in the porous region, $\beta=(\eta/\mu)/k$, k is a permeability of the porous material. The parameter β represents the ratio of microstructure size to the pore size. For the flow of couple stress fluid in the porous matrix, $\beta<<1$. Due to continuity of fluid in the porous matrix, the pressure p^* satisfies the Laplace equation

$$\frac{\partial^2 p^*}{\partial x^2}+\frac{\partial^2 p^*}{\partial y^2}+\frac{\partial^2 p^*}{\partial z^2}=0. \tag{32}$$

Integrating with respect to y over the porous layer thickness H and using the boundary condition of solid backing $\left(\frac{\partial p^*}{\partial y}=0\right)_{y=-H}$, we obtain

$$\left(\frac{\partial p^*}{\partial y}\right)_{y=0}=-\int_{-H}^{0}\left(\frac{\partial^2 p^*}{\partial x^2}+\frac{\partial^2 p^*}{\partial z^2}\right)dy. \tag{33}$$

Assuming the porous layer thickness H to be very small and using the continuity condition of pressure $(p=p^*)$ at the porous interface $(y=0)$, Eq. (33) reduces to

$$\left(\frac{\partial p^*}{\partial y}\right)_{y=0}=-H\left(\frac{\partial^2 p^*}{\partial x^2}+\frac{\partial^2 p^*}{\partial z^2}\right), \tag{34}$$

then the velocity component v_1 at the interface $(y=0)$ is given by

$$(v_1)_{y=0} = -\frac{kH}{\mu(1-\beta)}\left(\frac{\partial^2 p^*}{\partial x^2} + \frac{\partial^2 p^*}{\partial z^2}\right). \tag{35}$$

Substituting Eq. (35) in Eq. (27), the Dynamic Reynolds equation is obtained in the form

$$\frac{\partial}{\partial x}\left[\left\{f(h,l) + \frac{12kH}{(1-\beta)}\right\}\frac{\partial p}{\partial x}\right] + \frac{\partial}{\partial z}\left[\left\{f(h,l) + \frac{12kH}{(1-\beta)}\right\}\frac{\partial p}{\partial z}\right] = 12\mu\frac{\partial h}{\partial t}. \tag{36}$$

Introducing the non-dimensional quantities;

$$h_1 = \frac{h}{h_{m0}}, P = \frac{ph_{m0}^2}{LU\mu}, t_1 = \frac{Ut}{L}, x_1 = \frac{x}{L}, z_1 = \frac{z}{B}, \psi = \frac{kH}{h_{m0}^3},\ l_1 = \frac{l}{h_{m0}}\ . \tag{37}$$

After introducing the non-dimensional quantities, the dynamic Reynolds equation for the porous slider bearings can be expressed in a non-dimensional form as

$$\frac{\partial}{\partial x_1}\left[\left\{f_1(h_1,l_1) + \frac{12\psi}{(1-\beta)}\right\}\frac{\partial P}{\partial x_1}\right] + \frac{1}{\delta^2}\left[\left\{f_1(h_1,l_1) + \frac{12\psi}{(1-\beta)}\right\}\frac{\partial^2 P}{\partial z_1^2}\right] = 12\frac{\partial h_1}{\partial t_1}\ , \tag{38}$$

where

$$f_1(h_1,l_1) = h_1^3 - 12l_1^2h_1 + 24l_1^3\tanh\left(\frac{h_1}{2l_1}\right). \tag{39}$$

In the limiting case $\psi \to 0$, Eq. (38) reduces to the solid case studied by Lin, Lu and Chang (2003). To study the static and dynamic characteristics of the porous plane inclined slider bearing, the film thickness is separated into two parts: the minimum film thickness $h_m(t)$ and the slider profile function $h_s(x)$

$$h(x,t) = h_m(t) + h_s(x) = h_m(t) + a\left(1 - \frac{x}{L}\right)$$

where $a = h_1(t) - h_0(t)$, L is length of the bearing and its non-dimensional form is

$$h_1(x_1,t_1) = h_{1m}(t_1) + h_{1s}(x_1) = h_{1m}(t_1) + \lambda(1-x_1), \tag{40}$$

where $\lambda\left(=\frac{a}{h_{m0}}\right)$ is the slider-profile parameter.

The steady and dynamic characteristics of the porous bearings are obtained by using the perturbations in steady-state minimum film thickness at the outlet h_{m0}. The minimum film thickness and the local film pressure are assumed to be of the form

$$h_{1m} = 1 + \varepsilon e^{it_1},\ P = P_0 + P_1\varepsilon e^{it_1}, \tag{41}$$

where ε is the perturbation amplitude and is assumed to be small and $i = \sqrt{-1}$. Substituting into the dynamic Reynolds-type Eq. (38) and neglecting the higher

order terms of ε, the two Reynolds-type equations responsible for both steady-state pressure and the perturbed film pressure obtained are

$$\frac{\partial}{\partial x_1}\left[\left\{f_{10}(h_{1s},l_1)+\frac{12\psi}{(1-\beta)}\right\}\frac{\partial P_0}{\partial x_1}\right]+\frac{1}{\delta^2}\left\{f_{10}(h_{1s},l_1)+\frac{12\psi}{(1-\beta)}\right\}\frac{\partial^2 P_0}{\partial z_1^2}=-6\lambda\,, \quad (42)$$

$$\begin{aligned}&\frac{\partial}{\partial x_1}\left[f_{11}(h_{1s},l_1)\frac{\partial P_0}{\partial x_1}+\left\{f_{10}(h_{1s},l_1)+\frac{12\psi}{(1-\beta)}\right\}\frac{\partial P_1}{\partial \bar{x}}\right]+\\&\frac{1}{\delta^2}\left[f_{11}(h_{1s},l_1)\frac{\partial^2 P_0}{\partial z_1^2}+\left\{f_{10}(h_{1s},l_1)+\frac{12\psi}{(1-\beta)}\right\}\frac{\partial^2 P_1}{\partial z_1^2}\right]=12i\end{aligned} \quad (43)$$

where

$$f_{10}(h_{1s},l_1)=(1+h_{1s})^3-12{l_1}^2(1+h_{1s})+24{l_1}^3\tanh\left(\frac{1+h_{1s}}{2l_1}\right), \quad (44)$$

$$f_{11}(h_{1s},l_1)=3(1+h_{1s})^2-12{l_1}^2+12{l_1}^2\sec^2\mathrm{h}\left(\frac{1+h_{1s}}{2l_1}\right). \quad (45)$$

The boundary conditions for the steady state and perturbed film pressure are

$$P_0=0 \text{ at } x_1=0, x_1=1, z_1=0, z_1=1\,, \quad (46)$$

$$P_1=0 \text{ at } x_1=0, x_1=1, z_1=0, z_1=1\,. \quad (47)$$

The full Reynolds equation will be solved numerically by using a finite difference method (FDM). In finite increment format, the terms in the Eqs. (42) and (43) can be expressed as

$$\frac{\partial}{\partial x_1}\left[\left\{f_{10}+\frac{12\psi}{(1-\beta)}\right\}\frac{\partial P_0}{\partial x_1}\right]=\frac{1}{\Delta x_1}\left[\left(f_{10i+\frac{1}{2},j}+\frac{12\psi}{(1-\beta)}\right)\left\{\frac{P_{0i+1,j}-P_{0i,j}}{\Delta x_1}\right\}-\left(f_{10i-\frac{1}{2},j}+\frac{12\psi}{(1-\beta)}\right)\left\{\frac{P_{0i,j}-P_{0i-1,j}}{\Delta x_1}\right\}\right]$$

$$\left\{f_{10}+\frac{12\psi}{(1-\beta)}\right\}\frac{\partial^2 P_0}{\partial z_1^2}=\frac{1}{(\Delta z_1)^2}\left(f_{10i,j}+\frac{12\psi}{(1-\beta)}\right)\left\{P_{0i,j+1}-2P_{0i,j}+P_{0i,j-1}\right\},$$

$$\begin{aligned}\frac{\partial}{\partial x_1}\left[\left\{f_{10}+\frac{12\psi}{(1-\beta)}\right\}\frac{\partial P_1}{\partial x_1}+f_{11}\frac{\partial P_0}{\partial x_1}\right]&=\frac{1}{\Delta x_1}\left[\left(f_{10i+\frac{1}{2},j}+\frac{12\psi}{(1-\beta)}\right)\left\{\frac{P_{1i+1,j}-P_{1i,j}}{\Delta x_1}\right\}-\left(f_{10i-\frac{1}{2},j}+\frac{12\psi}{(1-\beta)}\right)\left\{\frac{P_{1i,j}-P_{1i-1,j}}{\Delta x_1}\right\}\right]\\&+\frac{1}{\Delta x_1}\left[f_{11i+\frac{1}{2},j}\left\{\frac{P_{0i+1,j}-P_{0i,j}}{\Delta x_1}\right\}-f_{11i-\frac{1}{2},j}\left\{\frac{P_{0i,j}-P_{0i-1,j}}{\Delta x_1}\right\}\right]\end{aligned}$$

and

$$\begin{aligned}\left\{f_{10}+\frac{12\psi}{(1-\beta)}\right\}\frac{\partial^2 P_1}{\partial z_1^2}+f_{11}\frac{\partial^2 P_0}{\partial z_1^2}&=\frac{1}{(\Delta z_1)^2}\left(f_{10i,j}+\frac{12\psi}{(1-\beta)}\right)\left\{P_{1i,j+1}-2P_{1i,j}+P_{1i,j-1}\right\}\\&+\frac{1}{(\Delta z_1)^2}f_{11i,j}\left\{P_{0i,j+1}-2P_{0i,j}+P_{0i,j-1}\right\}\end{aligned}$$

.

Substituting these expressions into the steady-state and perturbed Reynolds Eqs. (42) and (43), we get

$$P_{0i,j} = a_1 P_{0i+1,j} + a_2 P_{0i-1,j} + a_3 P_{0i,j+1} + a_4 P_{0i,j-1} + a_5 \tag{48}$$

$$\begin{aligned} P_{1rpi,j} &= a_1 P_{1rpi+1,j} + a_2 P_{1rpi-1,j} + a_3 P_{1rpi,j+1} + a_4 P_{1rpi,j-1} \\ &\quad + a_6 P_{0i+1,j} + a_7 P_{0i-1,j} + a_8 P_{0i,j+1} + a_9 P_{0i,j-1} + a_{10} P_{0i,j} \end{aligned} \tag{49}$$

$$P_{1ipi,j} = a_1 P_{1ipi+1,j} + a_2 P_{1ipi-1,j} + a_3 P_{1ipi,j+1} + a_4 P_{1ipi,j-1} + a_{11} \tag{50}$$

where the perturbed film pressure has been expressed in terms of real and imaginary parts, $P_1 = P_{1rp} + iP_{1ip}$.

The coefficients from a_0 to a_{11} be defined as

$$a_1 = \delta^2 b^2 \left(f_{10i+\frac{1}{2},j} + \frac{12\psi}{(1-\beta)} \right) \Big/ a_0$$

$$a_2 = \delta^2 b^2 \left(f_{10i-\frac{1}{2},j} + \frac{12\psi}{(1-\beta)} \right) \Big/ a_0$$

$$a_3 = a_4 = \left(f_{10i,j} + \frac{12\psi}{(1-\beta)} \right) \Big/ a_0$$

$$a_5 = 6\delta^2 \lambda (\Delta z_1)^2 \big/ a_0$$

$$a_6 = \delta^2 b^2 f_{11i+\frac{1}{2},j} \Big/ a_0$$

$$a_7 = \delta^2 b^2 f_{11i-\frac{1}{2},j} \Big/ a_0$$

$$a_8 = a_9 = \delta^2 b^2 f_{11i,j} \big/ a_0$$

$$a_{10} = -12\delta^2 \lambda (\Delta z_1)^2 \big/ a_0$$

$$a_{11} = \left[\delta^2 b^2 \left(f_{11i+\frac{1}{2},j} + f_{11i-\frac{1}{2},j} \right) + 2 f_{11i,j} \right] \Big/ a_0$$

where $a_0 = \delta^2 b^2 \left(f_{10i+\frac{1}{2},j} + \frac{12\psi}{(1-\beta)} + f_{10i-\frac{1}{2},j} + \frac{12\psi}{(1-\beta)} \right) + 2\left(f_{10i,j} + \frac{12\psi}{(1-\beta)} \right)$ (51)

and $b = \Delta z_1 / \Delta x_1$.

The steady-state pressure and perturbed film pressure are calculated by using FDM. The steady-state load capacity W_s and perturbed film force W_d are evaluated by integrating the steady-state film pressure and perturbed film pressure respectively over the film region.

$$Ws = \frac{\mu U L^2 B}{h_{m0}^2} \int_{x=0}^{x=L} \int_{z=0}^{z=B} p_0 dx dz \tag{52}$$

$$W_d = \frac{\mu U L^2 B}{h_{m0}^2} \int_{x=0}^{x=L} \int_{z=0}^{z=B} p_1 dx dz \tag{53}$$

where B is width of bearing and above equations are in non-dimensional form

$$Ws_1 = \frac{Wsh_{m0}^2}{\mu U L^2 B} = \int_{x_1=0}^{x_1=1} \int_{z_1=0}^{z_1=1} P_0 dx_1 dz_1 \approx \sum_{i=0}^{M} \sum_{j=0}^{M_1} P_{0i,j} \Delta x_1 \Delta z_1 \tag{54}$$

$$W_{d_1} = \frac{W_d h_{m0}^2}{\mu U L^2 B} = \int_{x_1=0}^{x_1=1} \int_{z_1=0}^{z_1=1} P_1 dx_1 dz_1 \approx \sum_{i=0}^{M} \sum_{j=0}^{M_1} P_{1i,j} \Delta x_1 \Delta z_1 \tag{55}$$

where $M+1$ and M_1+1 are the grid-point numbers in the x_1 and z_1 directions respectively, having $N=(M+1)\times(M_1+1)$ equations with N unknowns to determine. From the linear theory, the resulting dynamic film force can be expressed in terms of linearized spring and damping coefficients.

$$W_d \varepsilon e^{it_1} = -S_d h_{m0} \varepsilon e^{it_1} - C_d \frac{d}{dt_1}(h_{m0} \varepsilon e^{it_1}) \tag{56}$$

which is in non-dimensional form

$$W_{d_1} = -S_{d_1} - iC_{d_1} \tag{57}$$

where

$S_{d_1} = \frac{S_d h_{m0}^3}{\mu U L^2 B}$ and $C_{d_1} = \frac{C_d h_{m0}^3}{\mu L^3 B}$.

The dimensionless stiffness coefficient S_{d_1} and the damping coefficient C_{d_1} are obtained by equating the real and imaginary parts of W_{d_1} respectively as

$$S_{d_1} = -\mathrm{Re}(W_{d_1}) \approx -\sum_{i=0}^{M} \sum_{j=0}^{M_1} (P_{1rp})_{i,j} \Delta x_1 \Delta z_1 \tag{58}$$

$$C_{d_1} = -\mathrm{Im}(W_{d_1}) \approx -\sum_{i=0}^{M} \sum_{j=0}^{M_1} (P_{1ip})_{i,j} \Delta x_1 \Delta z_1 \tag{59}$$

4. Method of solution

From the system (48)-(50), we have

$$Au = b \tag{60}$$

where A is $N \times N$ coefficient matrix, b is $N \times 1$ matrix and u is $N \times 1$ matrix to be determined. By solving the Eq. (60) through the iterative method, we get the approximate solution v of u. i.e. $u = e + v \Rightarrow v = u - e$, where e is ($N \times 1$ matrix) error to be determined. In the numerical methods, approximate solution

containing some error. There are many approaches to minimize the error. Some of them are multigrid (MG), B-spline biorthogonal wavelet multigrid (BBWMG) and modified B-spline biorthogonal wavelet multigrid (MBBWMG) methods etc. Now, we are discussing about the method of solution of each, as follows.

4.1. Multigrid (MG) method

From Eq. (60), we get the approximate solution v of u. Now we find the residual as,

$$r_{N\times 1} = [b]_{N\times 1} - [A]_{N\times N}[v]_{N\times 1} \tag{61}$$

We reduce the matrices from the finer level to coarsest level using Restriction operator, i.e.

$$R = \frac{1}{4}\begin{pmatrix} 1 & 2 & 1 & 0 & 0 & \dots & 0 & 0 \\ 0 & 0 & 1 & 2 & 1 & \dots & 0 & 0 \\ \vdots & & \ddots & & & \dots & 0 & 0 \\ 0 & 0 & & \dots & & \dots & 1 & 2 \end{pmatrix}_{N/2\times N}$$

and then construct the matrices back to finer level from the coarsest level using Prolongation operator, i.e.

$$P = \frac{1}{2}\begin{pmatrix} 1 & 0 & 0 & \dots & 0 \\ 2 & 0 & 0 & \dots & 0 \\ 1 & 1 & 0 & \dots & \vdots \\ 0 & 2 & \vdots & \dots & \vdots \\ 0 & 1 & & & \\ \vdots & \vdots & \ddots & & \vdots \\ 0 & 0 & 0 & \dots & 1 \\ 0 & 0 & 0 & \dots & 2 \end{pmatrix}_{N\times N/2}.$$

From (14),

$$r_{N/2\times 1} = [R]_{N/2\times N}[r]_{N\times 1} \tag{62}$$

and $$[A]_{N/2\times N/2} = [R]_{N/2\times N}[A]_{N\times N}[P]_{N\times N/2}.$$

Residual equation becomes, $[A]_{N/2\times N/2}[e]_{N/2\times 1} = [r]_{N/2\times 1}$

where $e_{N/2\times 1}$ is to be determined. Solve $e_{N/2\times 1}$ with initial guess '0'.

From (15),

$$r_{N/4\times 1} = [R]_{N/4\times N/2}[r]_{N/2\times 1} \tag{63}$$

and $$[A]_{N/4\times N/4} = [R]_{N/4\times N/2}[A]_{N/2\times N/2}[P]_{N/2\times N/4}.$$

Then residual equation becomes, $[A]_{N/4\times N/4}[e]_{N/4\times 1} = [r]_{N/4\times 1}$.

Solve $e_{N/4\times 1}$ with initial guess '0'.

Continue the procedure up to the coarsest level, we have,

$$r_{1\times 1} = [R]_{1\times 2}[r]_{2\times 1} \tag{64}$$

and $$[A]_{1\times 1} = [R]_{1\times 2}[A]_{2\times 2}[P]_{2\times 1}.$$

Residual equation is, $[A]_{1\times 1}[e]_{1\times 1} = [r]_{1\times 1}$. Solve $e_{1\times 1}$ exactly. Now correct the solution

$$u_{2\times 1} = [e]_{2\times 1} + [P]_{2\times 1}[e]_{1\times 1}.$$

Solve $[A]_{2\times 2}[u]_{2\times 1} = [r]_{2\times 1}$ with initial guess $u_{2\times 1}$. Correct the solution

$$u_{4\times 1} = [e]_{4\times 1} + [P]_{4\times 2}[u]_{2\times 1}.$$

Solve $[A]_{4\times 4}[u]_{4\times 1} = [r]_{4\times 1}$ with initial guess $u_{4\times 1}$. Continue the procedure up to the finer level, Correct the solution

$$u_{N\times 1} = [v]_{N\times 1} + [P]_{N\times N/2}[u]_{N/2\times 1}.$$

Solve $[A]_{N\times N}[u]_{N\times 1} = [b]_{N\times 1}$ with initial guess $u_{N\times 1}$ and $u_{N\times 1}$ is the required solution of system (60).

4.2. B-spline biorthogonal wavelet multigrid (BBWMG) method

The same procedure is applied as explained in the case of MG method. Instead of using operators ' R ' and ' P ', here we use B-spline biorthogonal wavelet intergrid operators as,

B-spline biorthogonal wavelet restriction operator:

$$Bwr = \begin{pmatrix} h_{f0} & h_{f1} & h_{f2} & h_{f3} & 0 & 0 & \dots & 0 & 0 & h_{f-1} \\ g_{f0} & g_{f1} & 0 & 0 & 0 & 0 & \dots & 0 & 0 & g_{f-1} \\ 0 & h_{f-1} & h_{f0} & h_{f1} & h_{f2} & h_{f3} & 0 & \dots & 0 & 0 & 0 \\ 0 & g_{f-1} & g_{f0} & g_{f1} & 0 & 0 & \dots & 0 & 0 & 0 \\ \vdots & & \ddots & & \dots & & & \dots & 0 & 0 \\ 0 & 0 & \dots & 0 & g_{f-1} & g_{f0} & g_{f1} & 0 & \dots & 0 & 0 \end{pmatrix}_{\frac{N}{2}\times N} \quad \text{and}$$

B-spline biorthogonal wavelet prolongation operator:

$$Bwp = \begin{pmatrix} \tilde{h}_{f0} & \tilde{h}_{f1} & 0 & 0 & 0 & 0 & \dots & 0 & 0 & \tilde{h}_{f-1} \\ \tilde{g}_{f0} & \tilde{g}_{f1} & \tilde{g}_{f2} & \tilde{g}_{f3} & 0 & \dots & & 0 & 0 & \tilde{g}_{f-1} \\ 0 & \tilde{h}_{f-1} & \tilde{h}_{f0} & \tilde{h}_{f1} & 0 & 0 & \dots & 0 & 0 & 0 \\ 0 & \tilde{g}_{f-1} & \tilde{g}_{f0} & \tilde{g}_{f1} & \tilde{g}_{f2} & \tilde{g}_{f3} & 0 & \dots & 0 & 0 \\ \vdots & & \ddots & & \ddots & & \ddots & & & \vdots \\ 0 & \dots & 0 & 0 & \tilde{g}_{f-1} & \tilde{g}_{f0} & \tilde{g}_{f1} & \tilde{g}_{f2} & \tilde{g}_{f3} & \dots & 0 \end{pmatrix}^{T}_{\frac{N}{2}\times N}.$$

4.3. Modified B-spline biorthogonal wavelet multigrid (MBBWMG) method

Here also, same procedure is applied as explained in the above methods. Instead of using ‘ R ’ and ‘ P ’ matrices, here we use modified B-spline biorthogonal wavelet intergrid operators as,

Modified B-spline biorthogonal wavelet restriction operator:

$$MBwr = \begin{pmatrix} h_{f0} & 0 & h_{f1} & 0 & h_{f2} & 0 & h_{f3} & 0 & \dots & 0 & 0 & h_{f-1} & 0 \\ 0 & 1 & 0 & 0 & \dots & 0 & 0 & \dots & \dots & & & 0 & 0 \\ g_{f0} & 0 & g_{f1} & 0 & \dots & 0 & 0 & \dots & \dots & & 0 & g_{f-1} & 0 \\ 0 & 0 & 0 & 1 & 0 & \dots & 0 & 0 & \dots & \dots & & 0 & 0 \\ 0 & 0 & h_{f-1} & 0 & h_{f0} & 0 & h_{f1} & 0 & h_{f2} & 0 & h_{f3} & 0 & \dots & 0 & 0 \\ 0 & 0 & g_{f-1} & 0 & g_{f0} & 0 & g_{f1} & 0 & 0 & \dots & \dots & 0 & 0 \\ \vdots & & \ddots & & \ddots & & \ddots & & \dots & & \dots & & \ddots \\ 0 & 0 & \dots & 0 & g_{f-1} & 0 & g_{f0} & 0 & g_{f1} & 0 & 0 & \dots & 0 & 0 \end{pmatrix}_{\frac{N}{2}\times N} \quad \text{and}$$

Modified B-spline biorthogonal wavelet prolongation operator:

$$MBwp = \begin{pmatrix} \tilde{h}_{f0} & 0 & \tilde{h}_{f1} & 0 & 0 & 0 & \dots & 0 & 0 & \tilde{h}_{f-1} & 0 \\ 0 & 1 & 0 & 0 & \dots & 0 & 0 & \dots & \dots & 0 & 0 \\ \tilde{g}_{f0} & 0 & \tilde{g}_{f1} & 0 & \tilde{g}_{f2} & 0 & \tilde{g}_{f3} & \dots & 0 & 0 & \tilde{g}_{f-1} & 0 \\ 0 & 0 & 0 & 1 & 0 & 0 & \dots & \dots & 0 & 0 & 0 \\ 0 & 0 & \tilde{h}_{f-1} & 0 & \tilde{h}_{f0} & 0 & \tilde{h}_{f1} & 0 & \dots & 0 & 0 \\ \vdots & & \ddots & & \ddots & & \dots & & & & \vdots \\ 0 & \dots & 0 & \tilde{g}_{f-1} & 0 & \tilde{g}_{f0} & 0 & \tilde{g}_{f1} & 0 & \tilde{g}_{f2} & 0 & \tilde{g}_{f3} & 0 & \dots & \vdots \end{pmatrix}^{T}_{\frac{N}{2}\times N}.$$

5. Numerical implementation

In this section, the numerical solution of Reynolds equation is presented to show the applicability of the proposed scheme using B-spline biorthogonal wavelet

intergrid operators. But, first we consider the elliptic partial differential equation having exact solution, to show the efficiency of the method. The error is computed using $E_{\max} = \max|u_e - u_a|$, where u_e and u_a are exact and approximate solutions respectively.

Test Problem 5.1: First, consider the elliptic partial differential equation to show the efficiency of the method,

$$\frac{\partial^2 u}{\partial x^2} + \frac{\partial^2 u}{\partial y^2} + \frac{2\pi^2}{1+2\pi^2}\cos(\pi x)\cos(\pi y) = 0,\ -1 \le x, y \le 1 \tag{65}$$

subject to Dirichlet boundary conditions. The exact solution of the problem is given by $u(x,y) = \frac{1}{1+2\pi^2}\cos(\pi x)\cos(\pi y)$. As per the procedure explained in section 4, we obtained the results and are presented in comparison with exact solution in Figure 1 and the CPU time of the methods to obtain solutions with the maximum errors shown in Table 1.

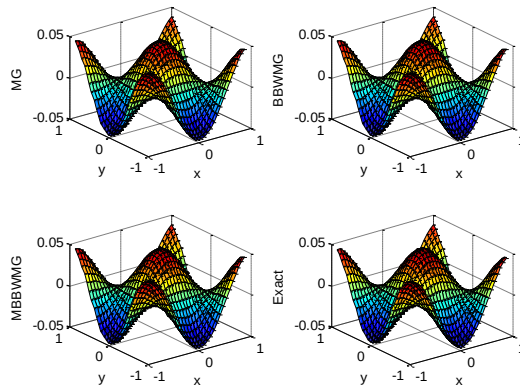

Figure 1. Comparison of numerical solutions with exact solution of test problem 5.1 for N=1024.

Table 1. Maximum error and CPU time (in seconds) of the methods of test problem 5.1.

N	Method	$E_{\max}$	Setup time	Running time	Total time
16	FDM	2.5315e-02	4.9355e+00	5.1811e-02	4.9873e+00
	MG	2.5315e-02	9.0954e-02	1.9914e-03	9.2946e-02
	BBWMG	2.5315e-02	2.8885e-02	1.8662e-03	3.0751e-02
	MBBWMG	2.5315e-02	2.1270e-02	1.5330e-03	2.2803e-02
64	FDM	9.0774e-03	3.9809e+00	5.1928e-02	4.0328e+00
	MG	9.0774e-03	8.8595e-02	3.1203e-03	9.1716e-02
	BBWMG	9.0774e-03	3.3945e-02	1.3185e-03	3.5264e-02
	MBBWMG	9.0774e-03	1.8182e-02	1.6291e-03	1.9811e-02

256	FDM	2.9092e-03	3.0990e+00	6.4944e-02	3.1640e+00
	MG	2.9092e-03	1.0625e-01	3.0143e-03	1.0927e-01
	BBWMG	2.9092e-03	1.2339e-01	1.0318e-03	1.2442e-01
	MBBWMG	2.9092e-03	2.4533e-02	1.7150e-03	2.6248e-02
1024	FDM	8.3080e-04	5.0385e+00	1.8907e-01	5.2276e+00
	MG	8.3079e-04	4.7867e-01	4.0125e-03	4.8268e-01
	BBWMG	8.3079e-04	3.7470e-01	2.5374e-03	3.7723e-01
	MBBWMG	8.3079e-04	1.4901e-01	2.6212e-03	1.5163e-01

Test Problem 5.2: Finally, consider the Reynolds equation, to show the applicability of the method, solving the system (3.33)-(3.35), we get both steady-state pressure P_0 and the perturbed film pressure P_1 and whose solutions are presented in the following figures for different parameters.

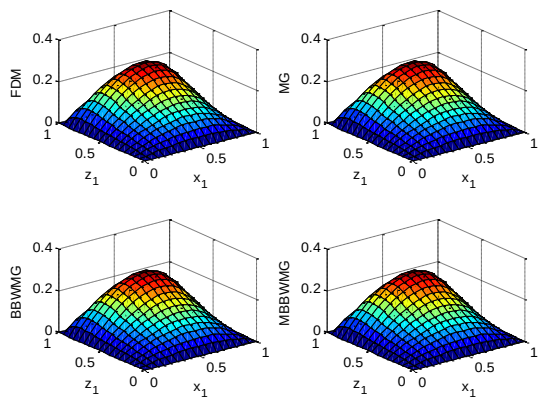

(a) l_1=0 (Newtonian)

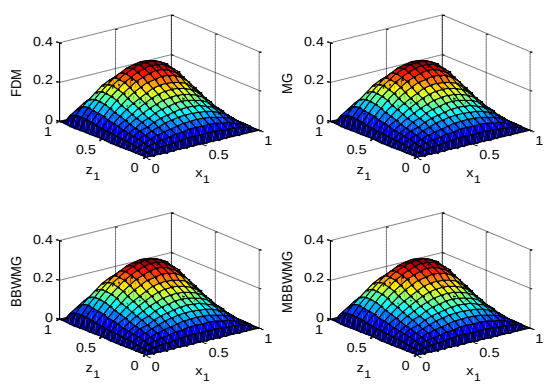

(b) l_1=0.1

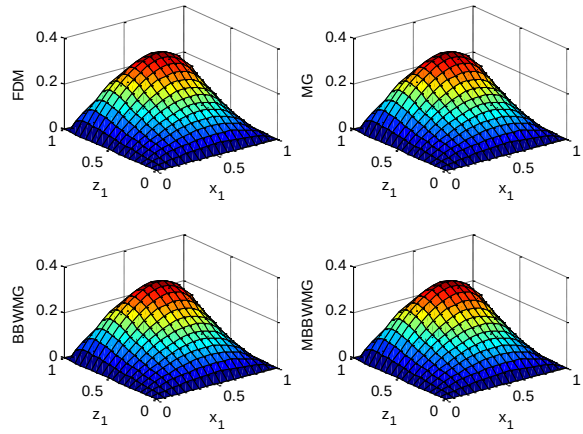

(c) l_1=0.2

Figure 2. Comparison of numerical solutions of steady-state pressure P_0 of test problem 5.2 for N=256 for $\lambda = 1.5$, $\delta = 2$, $\psi = 0.02$ and $\beta = 0.5$.

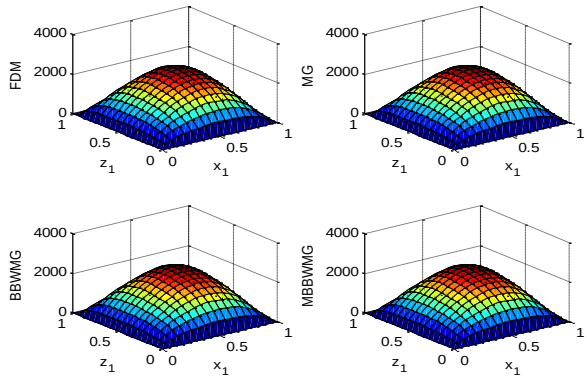

(a) l_1=0 (Newtonian)

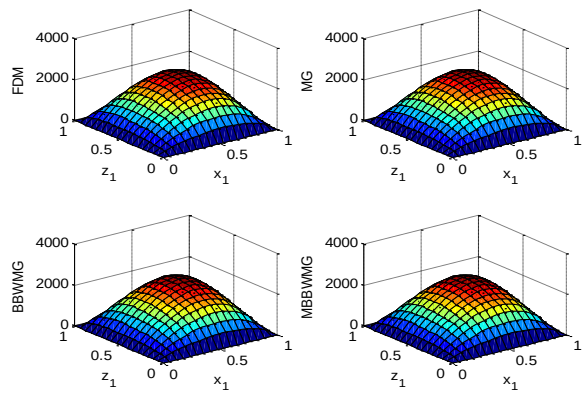

(b) l_1=0.1

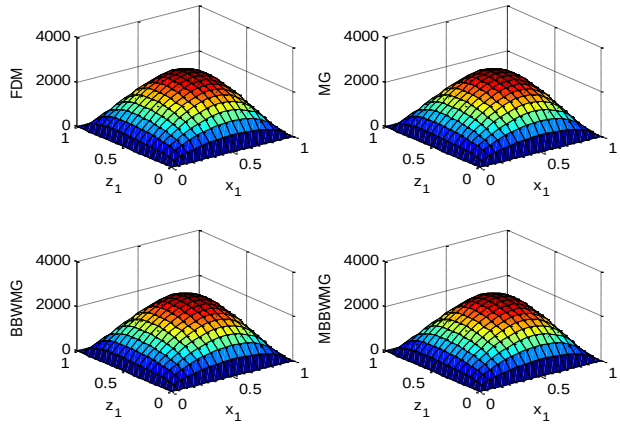

(c) l_1=0.2

Figure 3. Comparison of numerical solutions of perturbed film pressure P_1 of test problem 5.2 for N=256 for $\lambda = 1.5$, $\delta = 2$, $\psi = 0.02$ and $\beta = 0.5$.

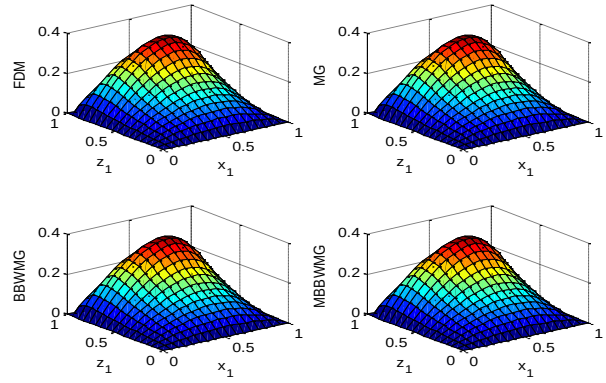

(a) $\psi = 0$ (Solid Case)

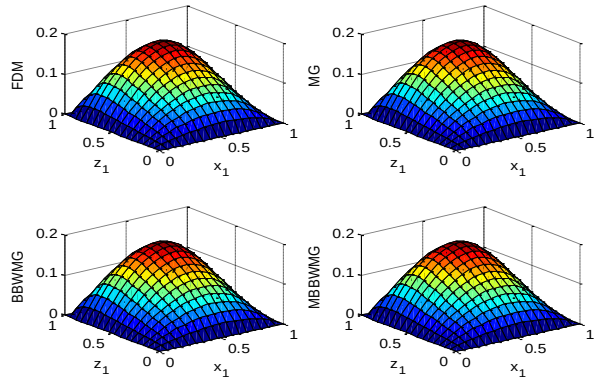

(b) $\psi = 0.1$

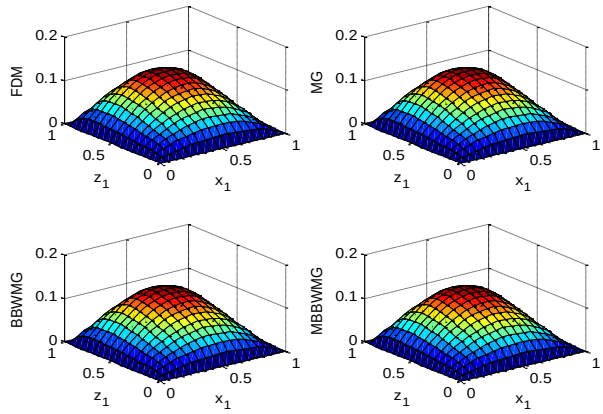

(c) $\psi = 0.2$

Figure 4. Comparison of numerical solutions of steady-state pressure P_0 of test problem 5.2 for N=256 for $\lambda = 1.5$, $\delta = 2$, $l_1 = 0.15$ and $\beta = 0.5$.

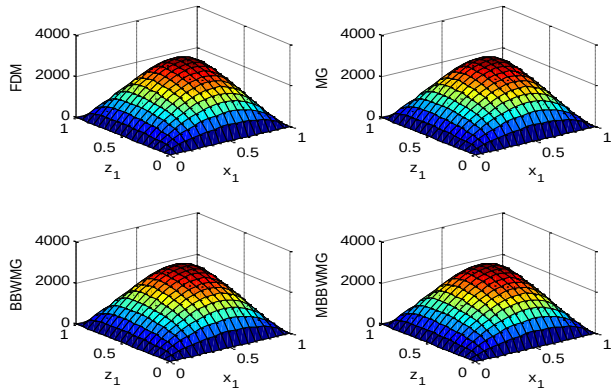

(a) $\psi = 0$ **(Solid Case)**

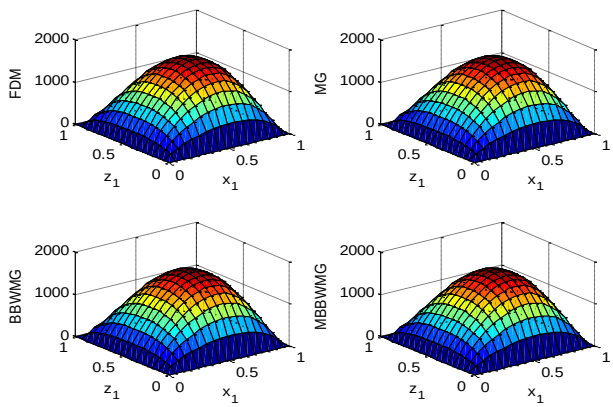

(b) $\psi = 0.1$

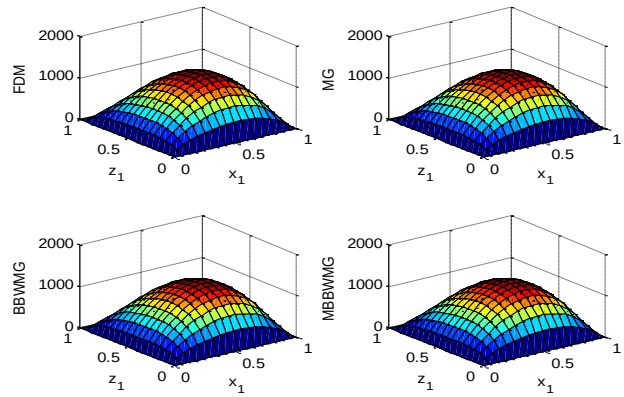

(c) $\psi = 0.2$

Figure 5. Comparison of numerical solutions of perturbed film pressure P_1 of test problem 5.2 for N=256 for $\lambda = 1.5$, $\delta = 2$, $l_1 = 0.15$ and $\beta = 0.5$.

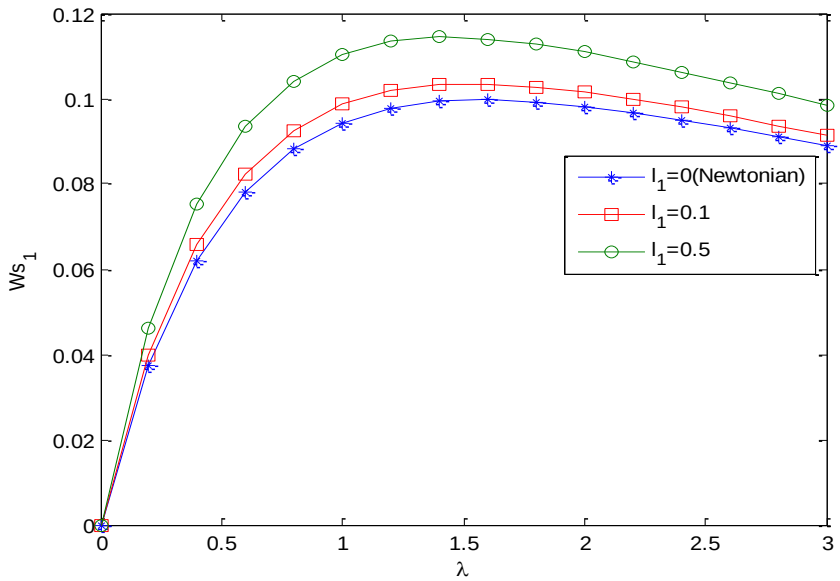

Figure 6. Variation of non-dimensional steady load-carrying capacity Ws_1 with profile parameter λ for N=256 for $\delta = 2$, $\psi = 0.02$ and $\beta = 0.5$.

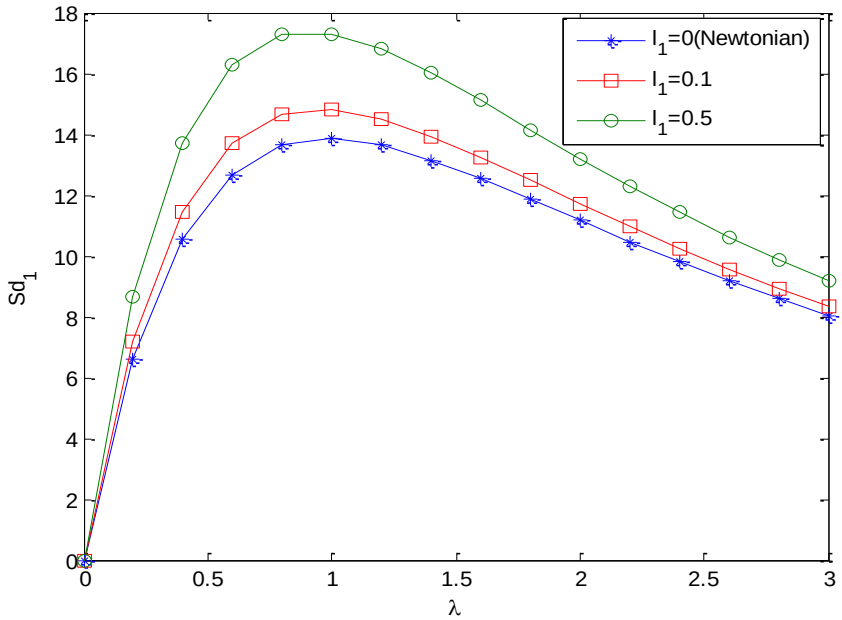

Figure 7. Variation of non-dimensional dynamic stiffness coefficient Sd_1 with profile parameter λ for N=256 for $\delta = 2$, $\psi = 0.02$ and $\beta = 0.5$.

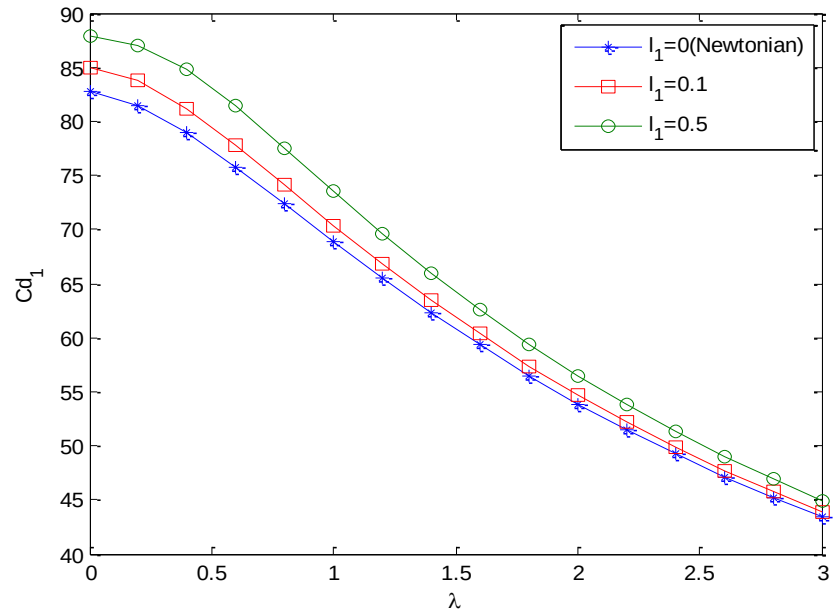

Figure 8. Variation of non-dimensional dynamic damping coefficient Cd_1 with profile parameter λ for N=256 for $\delta = 2$, $\psi = 0.02$ and $\beta = 0.5$.

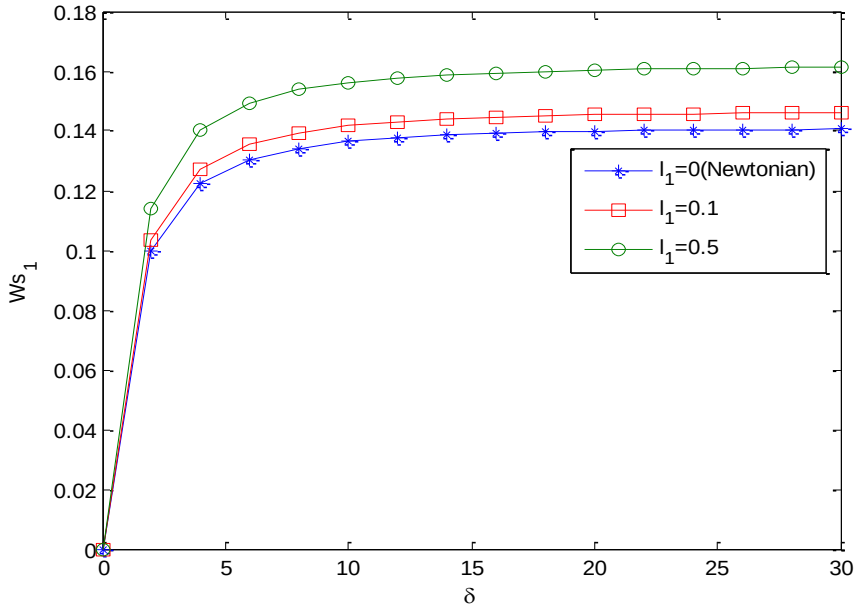

Figure 9. Variation of non-dimensional steady load-carrying capacity Ws_1 with aspect ratio δ for N=256 for $\lambda = 1.6$, $\psi = 0.02$ and $\beta = 0.5$.

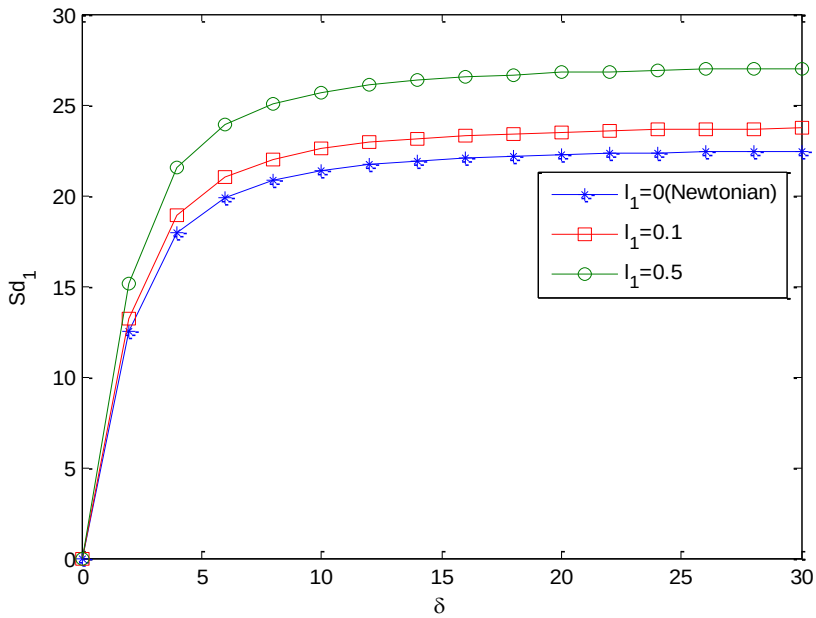

Figure 10. Variation of non-dimensional dynamic stiffness coefficient Sd_1 with aspect ratio δ for N=256 for $\lambda = 1.6$, $\psi = 0.02$ and $\beta = 0.5$.

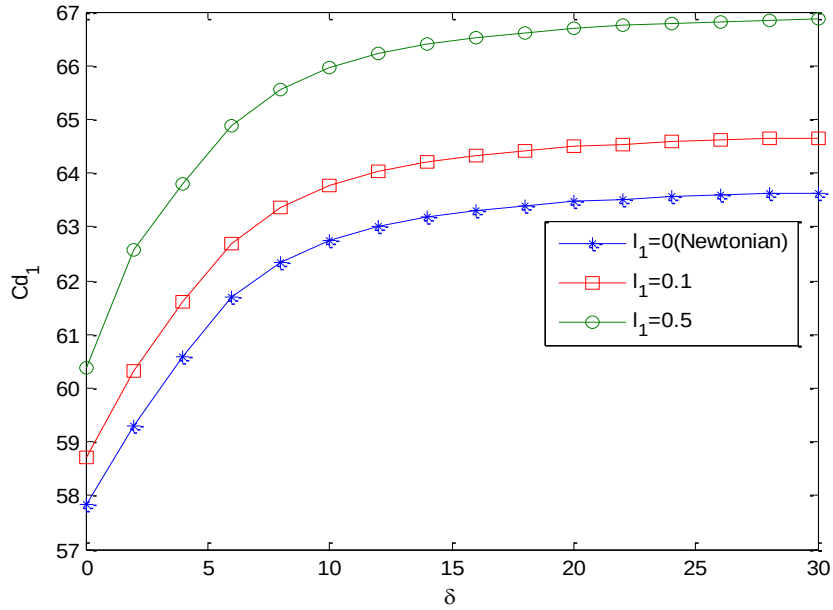

Figure 11. Variation of non-dimensional dynamic stiffness coefficient Cd_1 with aspect ratio δ for N=256 for $\lambda = 1.6$, $\psi = 0.02$ and $\beta = 0.5$.

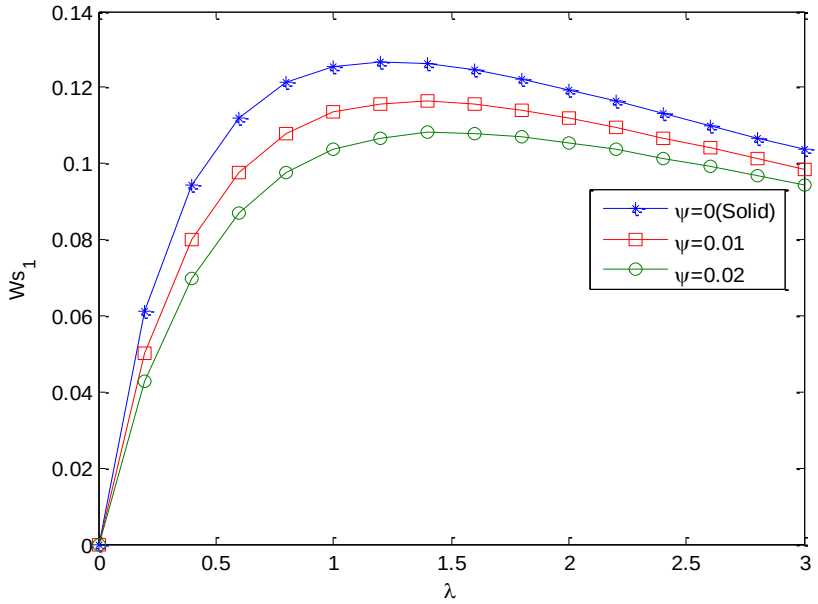

Figure 12. Variation of non-dimensional steady load-carrying capacity Ws_1 with profile parameter λ for N=256 for $\delta = 2$, $l_1 = 0.15$ and $\beta = 0.5$.

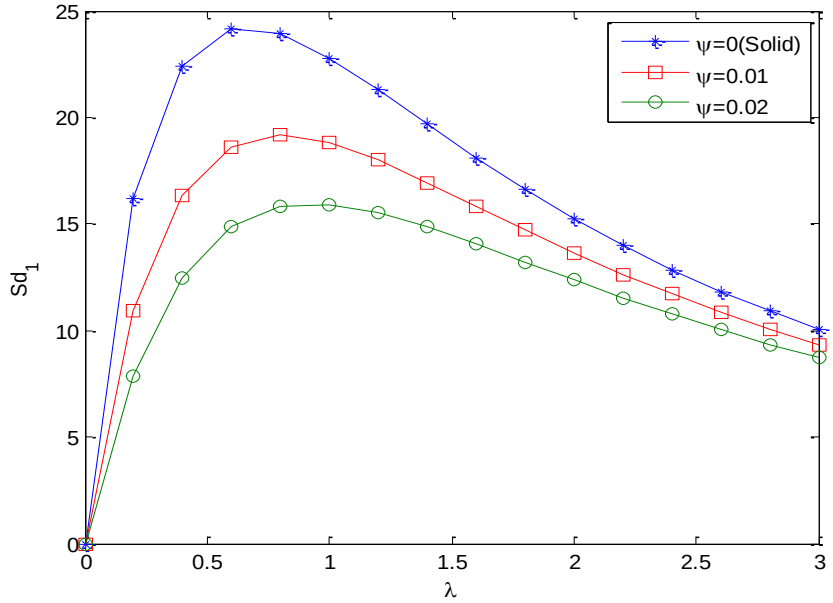

Figure 13. Variation of non-dimensional dynamic stiffness coefficient Sd_1 with profile parameter λ for N=256 for $\delta = 2$, $l_1 = 0.15$ and $\beta = 0.5$.

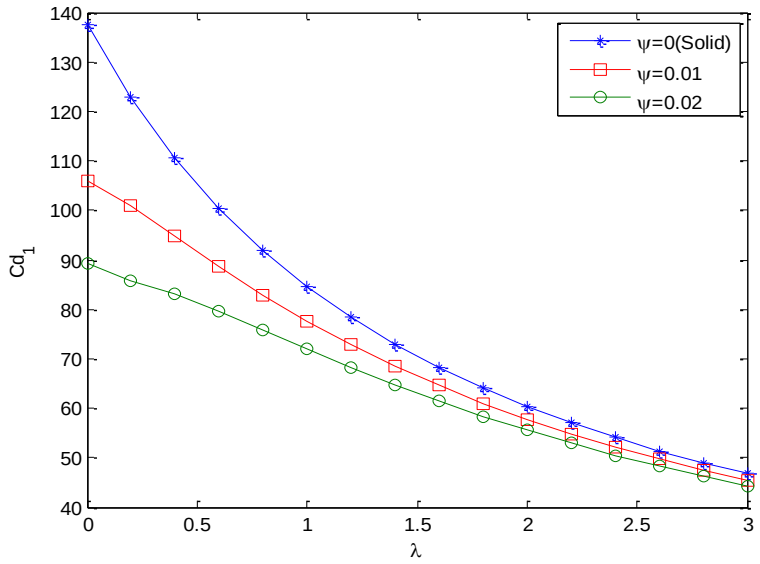

Figure 14. Variation of non-dimensional dynamic stiffness coefficient Cd_1 with profile parameter λ for N=256 for $\delta = 2$, $l_1 = 0.15$ and $\beta = 0.5$.

6. Results and discussion

Using the MatLab, results are obtained of the test problems. By observing results of the problem 1, numerical solutions are looking same with exact solution from the Figure 1 but the CPU time of the proposed scheme is better than the others, which is shown in the Table 1. Next switch on to lubrication problem, according to Stokes micro-continuum theory the new material parameter η in the Eqn. (3.1) is responsible for the property of couple stress. Therefore, the non dimensional couple stress parameter l_1 provides the mechanism of interaction of the fluid with the bearing geometry. It is expected that the couple stress effects are prominent either when the molecular size of additives is large or the minimum film thickness is small. *i. e.* when l_1 is large. The values of l_1 should be less than 1 for the validity of hydrodynamic lubrication *i. e*. the size of polar additives must be less than the minimum film thickness.

In this paper, with the aid of the non-dimensional parameter l_1, the effect of the couple stresses upon the steady-state performance and dynamic characteristics of infinitely wide inclined porous slider bearings is studied. The effect of the permeability on the static and dynamic characteristics of the bearings is analyzed through the permeability parameter ψ. When $\psi \rightarrow 0$, the modified Reynolds equation reduces to the solid case studied by Lin, Lu and Chang (2003). The variation of non-dimensional steady-state pressure P_0 and perturbed film pressure P_1 for different values of couple stress parameter l_1 are shown in the Figure 2 and Figure 3, respectively. It is observed that P_0 and P_1 increase by increasing values of l_1. The effect of permeability parameter ψ on the variation of P_0 and P_1 are depicted in the Figure 4 and Figure 5, respectively for the aspect ratio $\delta = 2$. It is observed that P_0 and P_1 decrease for increasing values of ψ.

The variation of non-dimensional steady-load carrying capacity Ws_1 with the profile parameter λ is presented in Figure 6 for different values of the couple stress parameter l_1. It is observed that, the effect of couple stress is to increase Ws_1 as compared to the corresponding Newtonian case ($l_1 = 0$). It is exciting to note that the existence of the critical value $\lambda_c = 1.4$ for the profile parameter λ at which Ws_1 attains maximum. Figure 7 shows the variation of non-dimensional dynamic stiffness coefficient Sd_1 with profile parameter λ for different values of l_1. It is observed that, the effect of couple stress is to increase Sd_1 as compared to the corresponding Newtonian case ($l_1 = 0$). Further, it is observed that, at the critical value $\lambda_c = 1.0$ of λ, Sd_1 attains the maximum value. The variation of non-dimensional dynamic damping coefficient Cd_1 with profile parameter λ for various values of l_1 is presented in Figure 8. It is observed that, the effect of couple stress on the Cd_1 is marginal for the larger values of λ. But there is a significant increase in the value of Cd_1 for the bearing under a smaller profile parameter. It is also observed that the significant reduction in Cd_1 by increasing the λ. Figure 9 depicts the variation of Ws_1 with aspect ratio δ for different values of l_1.

The rapid increase in Ws_1 is observed for smaller values of δ, whereas the marginal increase in Ws_1 is observed for larger values of δ ($\delta > 5$). Further it is observed that the couple stress fluid provides an increased Ws_1 as compared to the Newtonian case ($l_1 = 0$). The variation of Sd_1 with δ for various values of l_1 is shown in Figure 10. The sharp increase in Sd_1 is observed for smaller values of the aspect ratio δ

($0<\delta<5$) and the marginal increase in Sd_1 is obtained for larger values of δ. Figure 11 represents the variation of non-dimensional dynamic damping coefficient Cd_1 with aspect ratio δ for different values of l_1. It is observed that Cd_1 increases rapidly for smaller values of δ ($0<\delta<5$), though marginal increase in Cd_1 is observed for larger values of δ. Further, it is observed that the effect of couple stress is to increase Cd_1 as compared to the corresponding Newtonian case ($l_1=0$). The variation of Ws_1 with λ for different values of permeability parameter ψ is depicted in the Figure 12. It is observed that, the effect of ψ is to decrease Ws_1 as compared to the corresponding solid case ($\psi=0$). When the permeability is very high, the porous material becomes the main path of flow and hence decreases in Ws_1.

Further, it is observed that the critical value λ_c of λ, in which Ws_1 attains the maximum value. The value λ_c is a function of the permeability parameter ψ, increases by increasing ψ. The variation of non-dimensional dynamic stiffness coefficient Sd_1 with λ for different values of ψ is shown in the Figure 13. It is observed that as ψ increases, the value of Sd_1 decreases. Figure 14 represents the variation of non-dimensional dynamic damping coefficient Cd_1 with profile parameter λ for various values of ψ. It is observed that, the increase in the profile parameter λ, decreases in the value of Cd_1. Also, observed that the larger values of λ ($\lambda>2.0$) have marginal effect in the variations of Cd_1.

7. Conclusions

In this paper, we have introduced efficient B-spline biorthogonal wavelet multigrid schemes using intergrid operators based on B-spline biorthogonal wavelet filter coefficients. Here, we presented the numerical solution of Reynolds equation to show the applicability of the proposed scheme. To ensure the efficiency of the proposed scheme, first we considered the elliptic partial differential equation having exact solution. The efficiency and effectiveness of the proposed method is demonstrated through the results given tables and figures. Then, the proposed scheme is applied for the solution of Reynolds equation to show the applicability of the method. Hence the wavelet method is very convenient, efficient and has wide applications in the real world problems.

Acknowledgement

The authors thank to the UGC, New Delhi for the financial support of UGC's Research Fellowship in Science for Meritorious Students vide sanction letter no. F. 4-1/2006 (BSR)/7-101/2007 (BSR), dated-02/01/2013 during Ph. D time and also thank to KLECET, Chikodi for support to research.

References

1. Abduldaim A.M., Abdulrahaman A.A., Tahir F.S., The effectiveness of discrete hermite wavelet filters technique in digital image watermarking, Indonesian Journal of Electrical Engineering and Computer Science, V.25, N.3, (2022), pp.1392-1399.

2. Abdulrahaman A.A., Rasheed M., Shihab S., The Analytic of Image Processing Smoothing Spaces Using Wavelet, Journal of Physics: Conference Series, (2021), pp.1-15.
3. Abdulrahaman A.A., Tahir F.S., Face recognition using enhancement discrete wavelet transform based on MATLAB, Indonesian Journal of Electrical Engineering and Computer Science, V.23, N.2, (2021), pp.1128-1136.
4. Avudainayagam A., and Vani, C., Wavelet based multigrid methods for linear and nonlinear elliptic partial differential equations, Applied Mathematics and Computation, V.148, (2004), pp.307–320.
5. Beylkin G., Coifman R., Rokhlin V., Fast wavelet transforms and numerical algorithms-I, Communications in Pure and Applied Mathematics, V.44, (1991), pp.141-183.
6. Brandt A., Multi-level adaptive solutions to boundary-value problems, Mathematics of Computation, V.31, (1977), pp.333–390.
7. Briggs W.L., Henson V.E., McCormick S.F., A Multigrid Tutorial, SIAM: Philadelphia, (2000).
8. Bujurke N.M., Salimath C.S., Kudenatti R.B., and Shiralashetti S.C., Analysis of modified Reynolds equation using the wavelet-multigrid scheme, Numerical Methods for Partial Differential Equations: An International Journal, V.23, (2006), pp.692-705.
9. Bujurke N.M., Salimath C.S., Kudenatti, and Shiralashetti S.C., A fast wavelet- multigrid method to solve elliptic partial differential equations, Applied Mathematics and Computation, V.185, N.1, (2007), pp.667-680.
10. Bujurke N.M., Salimath C.S., Kudenatti R.B., and Shiralashetti S.C., Waveletmultigrid analysis of squeeze film characteristics of poroelastic bearings, Journal of computational and applied mathematics, V.203, (2007), pp.237-248.
11. Bulut F., Oruç Ö., Esen A., Higher order Haar wavelet method integrated with strang splitting for solving regularized long wave equation, Mathematics and Computers in Simulation, V.197, (2022), pp.277-290.
12. Bulut F., Oruç Ö., and Esen A., Numerical investigation of dynamic Euler-Bernoulli equation via 3-Scale Haar wavelet collocation method, Hacettepe Journal of Mathematics and Statistics, V.50, N.1, (2021), pp.159 – 179.
13. Deshi A.B., and Gudodagi G.A., Numerical solution of Nonlinear fractional differential equations using Haar wavelet collocation method, Fractals, V.29, N.6, (2021), pp.1-6.
14. Hackbusch W., Trottenberg U., Multigrid Methods, Springer-Verlag: Berlin, (1982).
15. Köse G.E., Oruç Ö., and Esen A., An application of Chebyshev wavelet method for the nonlinear time fractional Schrödinger equation, Mathematical Methods in the Applied Sciences, V.45, N.11, (2022), pp.6635-6649.

16. Lin J.R., Lu R.F., and Chang T.B., Derivation of dynamic couple stress Reynolds equation of sliding squeezing surfaces and numerical solution of plane inclined slide bearing, Tribology International, V.36, (2003), pp.679-685.
17. Luhmar M., Elastohydrodynamic analysis of double layered journal bearings with couple stress fluids, Proceedings of Institute of Mechanical Engineers Part-J: Journal of Engineering Tribology, V.219, (2005), pp.145-171.
18. Mohammed S.A., Abdulrahaman A.A., Tahir F.S., Emotions Students' Faces Recognition using Hybrid Deep Learning and Discrete Chebyshev Wavelet Transformations, International Journal of Mathematics and Computer Science, V.17, N.3, (2022), pp.1405-1417.
19. Naduvinamani N.B., Hiremath P.S., and Gurubasawaraj G., Squeeze film lubrication of a short porous journal bearing with couple stress fluids, Tribology International, V.34, (2001), pp.739-747.
20. Naduvinamani N.B., Hiremath P.S. and Gurubasawaraj G. Static and dynamic bearing of squeezing film lubrication of narrow porous journal bearings with couple stress fluid, Proceedings of Institute of Mechanical Engineers Part-J: Journal of Engineering Tribology, V.215, (2001), pp.45-62.
21. Naduvinamani N.B. and Marlai G.B. Numerical solution of couple stress full Reynolds equation for plane inclined porous slider bearings with squeezing effect, Canadian Journal of Pure and Applied Sciences, V.1, N.1, (2007), pp.83-96.
22. Naduvinamani N.B. and Patil S.B. Numerical solution of finite modified Reynolds equation for couple stress squeeze film lubrication porous journal bearings, Computers and Structures, V.87, (2009), pp.1287-1295.
23. Pinkus O., and Sternlicht B. Theory of hydrodynamic lubrication, McGraw-Hill, New York, (1961).
24. Ramanaih G., and Sarkar P. Squeeze films and thrust bearings lubricated by fluids with couple stress, Wear, V.48, (1978), pp.309-316.
25. Ramanaih G., and Sarkar P. Squeeze films between finite plates lubricated by fluids with couple stress, Wear, V.54, (1979), pp.315-320.
26. Ruch, D. K., and P. J. V. Fleet. Wavelet theory an elementary approach with applications. John Wiley and Sons: New Jersey, (2009).
27. Shiralashetti S.C., and Deshi A.B. An efficient Haar wavelet collocation method for the numerical solution of multi-term fractional differential equations, Nonlinear Dynamics, V.83, (2016), pp.293-303.
28. Shiralashetti S.C., Deshi A.B., and Mutalik Desai P.B. Haar wavelet collocation method for the numerical solution of singular initial value problems, Ain Shams Engineering Journal, V.7, (2016), pp.663–670.
29. Shiralashetti S.C., Kantli M.H., Deshi A.B., and Mutalik Desai P.B. A modified wavelet multigrid method for the numerical solution of

boundary value problems, Journal of Information and Optimization Science, V.38, N.1, (2017), pp.151-172.
30. Shiralashetti S.C., Kantli M.H., and Deshi A.B. Biorthogonal wavelet based full- approximation schemes for the numerical solution of elasto-hydrodynamic lubrication problems, Journal of Mathematical Modeling, V.6, N.1, (2018), pp.105-122.
31. Shiralashetti S.C., Angadi L.M., and Deshi A.B. Biorthogonal Wavelet Based Multigrid and Full Approximation Scheme for the Numerical Solution of Parabolic Partial Differential Equations, Asian-European Journal of Mathematics, V.12, N.1, (2019), pp.1-20.
32. Shiralashetti S.C., Kantli M.H., and Deshi A.B. Forthcoming. Daubechies modified wavelet multigrid method for the numerical solution of modified Reynolds equation for couple stress, Journal of Multiscale Modelling (Communicated).
33. Soman K. P., Ramachandran K.I. Insight in to wavelets, form theory to practice, Prentice Hall, India, (2005).
34. Stokes V.K. Couple stresses in fluids, The physics of fluids, V.9, (1966), pp.1709-1715.
35. Sweldens W. The construction and application of wavelets in numerical analysis, Ph. D. Thesis, Department of Computer Science, Katholieke Universiteit Leuven, Belgium, (1994).
36. Tahir F.S., Abdulrahaman A.A., Thanon Z.H. Novel face detection algorithm with a mask on neural network training, international journal of nonlinear analysis and applications, V.13, N.1, (2022), pp.209-215.
37. Trottenberg U., Oosterlee C. and Schuller A. Multigrid, Academic Press, London, (2001).
38. Wesseling P. An Introduction to Multigrid Methods, John Wiley, Chichester, (1992).